Open access • Journal Article • DOI:10.1346/CCMN.2016.0640411

Intercalation of ethylene glycol in smectites: several molecular simulation models verified by x-ray diffraction data — Source link

Marek Szczerba, Andrey G. Kalinichev

Institutions: Polish Academy of Sciences, École des mines de Nantes

Published on: 01 Aug 2016 - Clays and Clay Minerals (GeoScienceWorld)

INTERCALATION OF ETHYLENE GLYCOL IN SMECTITES: SEVERAL MOLECULAR SIMULATION MODELS VERIFIED BY X-RAY DIFFRACTION DATA

Marek Szczerba, Andrey G. Kalinichev

Intercalation of ethylene glycol in smectites: Several molecular simulation models verified by X-ray diffraction data

Marek Szczerba[1,*], Andrey G. Kalinichev[2]

[1] Institute of Geological Sciences, Polish Academy of Sciences, Kraków, Poland

[2] Laboratoire SUBATECH (UMR 6457), Ecole des Mines de Nantes, Nantes, France

[*)] Corresponding author: ndszczer@cyf-kr.edu.pl

KEY WORDS: Ethylene glycol, Smectite, Molecular dynamics, X-ray diffraction

ABSTRACT

Organo-clays represent a special challenge for molecular simulations, because they require accurate representation of the clay part and the organic/aqueous part of the model system and an accurate representation of their interactions. Due to a broad diversity of available force field models, it is an important question which sets of parameters will best suit the molecular modeling of the organo-intercalated smectites. To address this question, we use the structure of ethylene glycol (EG)-smectite complex as a testing model, because the intercalation of EG in smectites provides a stable interlayer complex with relatively constant basal spacing.

Three smectite samples with substantially different layer charge and charge localization were selected for X-ray diffraction (XRD) measurements. Their molecular models were built and molecular dynamics simulations were performed using various

combinations of the organic force fields (CGenFF, GAFF, CVFF and OPLS-aa) with ClayFF and INTERFACE force fields used to describe smectites. The simulations covered a range of different EG and water contents in the selected smectites. For every structure, the density distribution of interlayer species along the direction perpendicular to the layer plane was calculated and then used to optimize the X-ray diffraction patterns for these simulated models.

A comparison of these results with experimental XRD patterns shows very large discrepancies in the obtained structures and basal spacings for different layer charges as well as for different force fields and their combinations. The most important factor affecting the accuracy of the calculated diffractograms is found to be the selection of the clay mineral force field parameters. The second important conclusion is that a slight modification of the basal oxygen parameters for non-electrostatic interactions (increase of their effective atomic diameters) may be a simple and straightforward way to greatly improve the agreement of the modeled diffractograms with experiments, especially for high-charge smectites. Generally, among the organic force fields the least accurate results are obtained with CGenFF. For unmodified ClayFF, its combination with GAFF gives the best results, while the two other sets (OPLS-aa and CVFF) give the best results in combination with ClayFFmod. The INTERFACE and INTERFACEmod force fields are found to be producing much better results for low-charge montmorillonite than for high-charge smectites.

INTRODUCTION

Recent growing interest in organo-clay nanocomposites is clearly reflected in the development of computational molecular modeling approaches to quantitative understanding of the structural and dynamic behavior of such systems (e.g. Zeng *et al.*, 2003; Suter and Coveney, 2009; Suter *et al.*, 2011, 2015; Greathouse *et al.*, 2014; Heinz and Ramezani-Dakhel, 2016). Apart from the atomistic structural data necessary to construct the molecular models, the most fundamental information required to perform such simulations is contained in the sets of parameters describing interatomic interactions in the modeled systems, often collectively called the *force fields*. The fact that in the literature there are currently several widely used and well tested classical force fields available for molecular modeling of clays and related inorganic materials (e.g. Heinz *et al.*, 2005) and even a larger number of various force fields for molecular simulations of organic and bio-organic molecules (e.g. Guvench and MacKerell, 2008), often leaves unanswered the important question of finding an optimal combination of the force field parameters for accurate molecular modeling of both the organic and inorganic parts of the composite systems. Indeed, estimating the actual predictive capabilities of such simulations is a highly non-trivial task. In order to quantitatively address this issue one needs a testing model which should be known to provide a stable interlayer complex, and should be supported by sufficient amount of reliable experimental data for comparisons with the simulated results. For these reasons, complexes of smectites with ethylene glycol (EG)-water mixtures were selected for the present study.

Intercalation of EG in hydrated divalent ion-smectites is known to provide a structure with relatively constant basal spacing (e.g. Mosser-Ruck *et al.*, 2005). During this process, EG molecules penetrate into the interlayer spaces of the swelling clays, leading to the formation of a two-layer structure (d ~ 17 Å). For the purpose of X-ray diffraction data interpretation, a simplified model of this complex has been proposed by Reynolds (1965).

Further studies have shown that the basal spacing is larger for clay minerals with lower layer charge, but it also depends on the localization of the charge, the type of the exchangeable cations, the particle size and the relative humidity (Harward and Brindley, 1965; Brindley, 1966; Harward *et al.*, 1969; Środoń, 1980; Sato *et al.*, 1992). If the charge is located in the tetrahedral sheet then the values of basal spacing are lower than those observed when the charge is located in the octahedral sheet (Sato *et al.*, 1992). Later studies have shown that smectites may form a one-layer EG complex instead of the two-layer complex at very low relative humidities (Eberl *et al.*, 1987), or with K^+ as the exchange cation even at intermediate humidities (Eberl *et al.*, 1986). The experimental observations were to some extent explained with the help of molecular simulations, e.g. the preference of formation of bilayer structure and the preferred number of water molecules in the structure for the Ca^{2+} form (Szczerba *et al.*, 2014). Several methods of clay glycolation with specific technicalities are possible and Mosser-Ruck *et al.* (2005) have demonstrated certain differences and inconsistencies between them. The formation of monolayer or bilayer complexes was found to be dependent on the type of the interlayer cation and the concentration of EG in the close vicinity around smectite (the glycolation protocol). There is also a gradual loss of EG from the complex with smectite because of the equilibration between the complex and the surrounding environment. Therefore, X-ray measurements on such samples should be performed relatively quickly, within a few hours after glycolation. The dynamics of EG intercalation into smectites was studied by Svensson and Hansen (2010) using synchrotron X-ray diffraction techniques. This study showed that EG molecules replace H_2O in the interlayer, however, still leaving significant amounts of water in the structure.

The present study was undertaken in order to investigate the effects of different combinations of force field parameters on the accuracy of two-EG layer structure

representation. For this purpose inorganic (clay) and organic (EG) force field parameters need to be coupled in one simulation.

For clay minerals there exist several force field parameterizations that were used for molecular simulations of these structures over the past three decades. These parameters can be preliminarily divided into two groups: the ones that rely on the assumption of a rigid clay framework and the ones allowing partial orfull flexibility of the structure. Historically, the parametrizations of the first kind were developed earlier (e.g. Skipper *et al.*, 1991; Smith, 1998). They are, however, inherently limited and can lead to incorrect representation of the processes of adsorption, surface hydration, hydrogen bonding, diffusion rates etc. (e.g. Cygan *et al.*, 2009). The flexible force field parameterizations are currently much wideer represented (e.g. Hill and Sauer, 1995; Teppen *et al.*, 1997; Sato *et al.*, 2001; Manevitch and Ruthlege, 2004, Cygan *et al.*, 2004; Heinz *et al.*, 2005). It was shown, however, that only the parametrizations of Heinz *et al*. (2005) and ClayFF (Cygan *et al.*, 2004) give cleavage energies that reasonably correspond to the experimental values (Heinz *et al.*, 2005). Therefore, only these force fields were tested in this study. Additionally, Ferrage *et al*. (2011) have shown that a better description of the hydrated interlayer structure with the ClayFF force field can be achieved if the Lennard-Jones parameters of clay surface oxygens are increased by ~7%.

The interatomic interaction parameters for EG can be selected from a wide range of different organic force fields. Usually, these force fields are parameterized to optimize the description of certain specific sets of organic molecules. For example, CHARMM was constructed to model proteins (MacKerrel *et al.*, 1998), AMBER – to model peptides, proteins and nucleic acids (Cornell *et al.*, 1995), OPLS-aa for simulations of liquid hydrocarbons (Jorgensen *et al.*, 1996) and CVFF for amino acids, hydrocarbons, and many other organic molecules (Dauber-Osguthorpe *et al.*, 1988). More recent parameterizations which belong to a

120 certain earlier family but were later re-optimized for a larger set of organic molecules include
121 CHARMM-related CGenFF (general force field for drug-like molecules; Vanommeslaeghe *et*
122 *al.*, 2009) and AMBER-related GAFF (general AMBER force field; Wang *et al.*, 2004). For
123 the purpose of this study the parametrization of a given family that was best optimized for
124 small organic molecules, such as EG, was taken into account.

125 Even a more diverse set of force field parameterizations for water molecules are
126 available in the literature (e.g. Wallqvist and Mountain, 1999; Guillot, 2002; Kalinichev,
127 2001). In this study only the SPC (simple point charge)model of Berendsen *et al.* (1981) is
128 considered because it is known to perform well in combination with ClayFF, gives relatively
129 good solution structure for smectite interfaces and interlayers (e.g. Heinz *et al.*, 2005; Morrow
130 *et al.*, 2013; Ngouana-Wakou and Kalinichev, 2014; Greathouse *et al.*, 2015) and is also
131 consistent with the CVFF and INTERFACE parametrizations. Thoretically, the application of
132 different force field parametrizations for H_2O molecules can affect the simulation results for
133 hydrated clays. The work of Ferrage *et al.* (2011) has shown, however, that using the SPC
134 model is sensible in terms of the agreement of MD simulation results with X-ray diffraction
135 data.

136 Hybrid organo-clay materials is a rapidly growing area of molecular simulation studies
137 that requires a reliable coupling of different force field parameters. Very often ClayFF is used
138 together with CVFF (e.g. Kumar *et al.*, 2006; Liu *et al.*, 2007; Suter and Coveney, 2009;
139 Kalinichev *et al.*, 2010). There are also examples of successful use of ClayFF in combination
140 with OPLS-aa (e.g. Schampera *et al.*, 2015), CHARMM (e.g. Duque-Redondo *et al.*, 2014)
141 and AMBER (e.g. Wang et al., 2014; Swadling *et al.*, 2010). INTERFACE force field (Heinz
142 *et al.*, 2013) is also recently developed to be used in the studies of interactions of organic
143 molecules with minerals, including smectite clays, together with CVFF, PCFF and
144 COMPASS organic parameterizations. There are also other examples of combinations of

older clay mineral force field parameters with different organic force fields: e.g. Tambach *et al*. (2006) used force field of Skipper *et al*. (1995) together with OPLS-ua (Jorgensen *et al.*, 1986). Not all of these earlier force field combinations were extensively tested before they we used in this area of very active current research.

At the same time, the structures obtained from molecular simulations using different force field parameters can be validated by their comparison with available X-ray diffraction data. This methodology has been widely used for hydrated clay minerals (e.g. Ferrage *et al.*, 2011). Even though only the atomic density distribution of the interlayer species along a direction perpendicular to the layering plane can be considered for turbostratic smectites, it is still a very powerful methodology. It was used in the present study for the purpose of finding the optimal set of force field parameters for organic molecules interacting with smectites.

METHODOLOGY

Smectite samples used in the study

Three smectite samples from the collection of the Source Clays Repository of The Clay Minerals Society were studied. They have crystal structures with notably different layer charge and charge localization: low charge montmorillonite (SWy-1), high charge montmorillonite (SAz-1), and high charge beidellite (SbCa-1). Some of their characteristics are summarized in Table 1.

=== Table 1 ===

The particle size fractions were separated to avoid contamination with phases other than smectite. All samples were studied in Ca^{2+} form that was prepared via dialysis.

The samples were sedimented from aqueous solution on a glass slide. Then all slides were glycolated with the following procedure: each air-dried sample from RH around 50% was put into a closed plastic box (15×15×3 cm) that was placed in a vessel with EG solution poured at the bottom. The sample within the box was heated at 60 ºC for 10 h in an oven.

XRD patterns registration

To minimize EG loss from the prepared EG-smectite complexes the XRD patterns for all samples were measured directly after glycolation and in EG-saturated atmosphere. The X-ray diffraction datawere collected in the range from 2º to 60º 2Θ using a *Thermo ARL* XRD system, CuK_{α} radiation, and a Peltier-cooled solid-state detector. The tube current and voltage were 45 mA and 35 kV, respectively. The following slit sizes from tube to detector were used: 0.9 mm (0.645º), 1.3º Soller, 1.05 mm, sample, 1.0 mm, 1.3º Soller, 0.3 mm. The step size was 0.05º and the counting time was 20 s per step.

Molecular dynamics simulations

The simulated structural models of smectites were based on the pyrophyllite crystallographic data (Lee and Guggenheim, 1981), with several isomorphic substitutions introduced at particular atomic sites to mimic the experimentally studied smectite samples. All three structures were built by substituting a relevant number of Al atoms with Mg and Si with Al in the octahedral and tetrahedral sheets of the clay structure, respectively. The Mg/Al ordering in the octahedral sheets was introduced following the work of Ortega-Castro *et al.* (2010), *i.e.* maximizing the distance between Mg atoms. The Al/Si ordering in the tetrahedral sheet was random but obeying the Löwenstein rule, *i.e.* exluding Al-O-Al linkages. The simulation supercell was 8×4×2 unit cells in the *a*, *b*, and *c* crystallographic directions,

194 respectively (~41.6 Å × 36.1 Å × Z Å; the value of Z varied depending on the amount of EG
195 and H_2O in the interlayer space and the force field used).

196 The total energy of a molecular model is usually described by a sum of Coulombic
197 (electrostatic) interactions, short-range non-electrostatic interactions (sometimes referred to as
198 the Van der Waals terms), and bonded (intramolecular) interactions:

199 $$E_{Total} = E_{Coul} + E_{VDW} + E_{Bonded} \quad (1)$$

200 The bonded terms are especially important for organic molecules and typically include the
201 bond stretching, angle bending energy terms, various torsional terms, etc. The electrostatic
202 energy is represented by Coulomb's law:

203 $$E_{Coul} = \frac{e^2}{4\pi\varepsilon_o} \sum_{i \neq j} \frac{q_i q_j}{r_{ij}} , \quad (2)$$

204 where r_{ij} is the separation distance between the charged atoms i and j, e is the charge of the
205 electron, ε_o is the dielectric permittivity of vacuum (8.85419×10^{-12} F/m), and the partial
206 charges q_i and q_j are usually derived from quantum mechanics calculations and assigned by
207 the specific force field model. The Van der Waals energy term is usually represented by the
208 conventional Lennard-Jones (12-6) function, and includes the short-range repulsion associated
209 with the increase in energy as two atoms closely approach each other and the attractive
210 dispersion energy:

211 $$E_{VDW} = \sum_{i \neq j} D_{o,ij} \left[\left(\frac{R_{o,ij}}{r_{ij}} \right)^{12} - 2 \left(\frac{R_{o,ij}}{r_{ij}} \right)^{6} \right] . \quad (3)$$

212 $D_{o,ij}$ and $R_{o,ij}$ are empirical parameters specific to a particular force field model. The
213 interaction parameters between the unlike atoms are usually calculated according to the so-
214 called Lorentz-Berthelot mixing rules (e.g. Allen and Tildesley, 1987): arithmetic mean for
215 the distance parameter, R_o, and the geometric mean for the energy parameter, D_o:

216 $$R_{o,ij} = \tfrac{1}{2} (R_{o,i} + R_{o,j}) \quad (4)$$

$$D_{o,ij} = \sqrt{D_{o,i} D_{o,j}} \quad (5)$$

The Coulombic and VDW interactions are excluded for proximate intramolecular (bonded) interactions (i.e., 1-2 and 1-3 atom position exclusions) when large organic molecules are modeled.

In our case, the interatomic interactions involving smectite structures were described with the ClayFF (Cygan *et al.*, 2004) and the INTERFACE (Heinz *et al.*, 2005) force fields. GAFF, OPLS-aa, CGenFF, and CVFF organic force fields were used for EG, while the SPC model was assumed for water molecules (Berendsen *et al.*, 1981). The INTERFACE force field was only coupled with the CVFF organic force field because of the consistency of its 1-4-scaling factors (value of 1.0). CGenFF assumes no scaling, while OPLS-aa uses a scaling factor of 0.5, and GAFF uses 0.5 for the non-bonded non-electrostatic part of the interaction and 0.8333 for the electrostatic interactions. ClayFF has no restrictions on the organic force field that it can be coupled with, because no 1-4 pairs are present in this parametrization. Additionally, in the original clay mineral force fields, the Lennard-Jones parameters for basal oxygens, O_b, were modified as suggested by Ferrage *et al.* (2011) (ClayFFmod and INTERFACEmod). The LJ parameters of tetrahedral Si and Al atoms were, respectively, also modified in these models to maintain the same Si-O_b and Al-O_b distances as in the original force fields (see Szczerba *et al.*, 2016 and supplementary materials for a more detailed discussion). Ewald summation was applied to calculate the long range corrections to the Coulombic interactions (e.g., Allen and Tildesley, 1987) and the cut-off distance was set to 8.5 Å.

A set of different EG compositions around those of Reynolds (1965) – 1.7 EG per half unit cell (phuc) – was covered by the simulations to obtain the basal spacing closest to the experimentally observable. A constant number of interlayer water molecules – 0.8 H_2O phuc – was assumed. Additionally, for the set of parameters that gave the best results in previous

calculations, the EG content was set to vary from 1.4 to 2.0 with a step of 0.2 phuc, while the water content also varied between 0.0 and 1.2 H_2O phuc with a step of 0.3 phuc.

For all models, structural optimizations (total energy minimizations) were performed first, followed by *NPT*-ensemble MD simulations at 1 bar under evolving temperature using a Langevin dynamics algorithm to control the temperature and a Langevin piston to control the pressure. The time step to integrate the equations of atomic motion was set to 1 fs and the dynamic trajectories of all atoms and system properties were recorded every 1 ps. For the first 0.5 ns the temperature was set to 398 K. Then the temperature dropped to 298 K and the simulation continued for 1 ns. From the last 0.5 ns the equilibrium system properties were recorded for further analysis. To exclude any undesirable displacement of the center of mass of the simulated model, in all simulations one atom of the octahedral sheet was fixed at its initial position, but its interactions with all neighboring atoms were still fully accounted for. All MD simulations were performed using the LAMMPS computer program (Plimpton, 1995; http://lammps.sandia.gov).

Parametrization of EG molecules with organic force fields

CGenFF parameters were automatically assigned with the help of the on-line tool (cgenff.paramchem.org) using the NAMD convention, which was modified to make it consistent with the LAMMPS format. GAFF parametrization was performed using the *moltemplate* program (moltemplate.org) with charges automatically assigned using the program *TPACM4* available at www.scfbio-iitd.res.in/software/drugdesign/charge.jsp (Mukherjee *et al.*, 2011). CVFF parameters were automatically assigned within this force field's implementation in the LAMMPS program. Partial atomic charges were calculated based on the bond increments from the file containing CVFF parameters. OPLS-aa parameters were also automatically assigned using the *moltemplate* program. Tcl scripts executed in the

267 VMD molecular visualization program (Humphrey *et al.*, 1996) were used to generate all
268 input files for LAMMPS simulations.
269
270 ***Calculation of the simulated XRD patterns***
271 For every simulated structure, the atomic density distributions of the interlayer species
272 as well as electron density profiles along the direction perpendicular to the layering were
273 calculated. Then all the distributions were symmetrized with respect to the interlayer center
274 and used as an input for calculations of the X-ray diffraction patterns using the Sybilla code
275 (Chevron proprietary). The values of T_{mean}, *d*-spacing, σ^* and Δ-*d*-spacing were optimized
276 automatically. The range of $2\theta < 4.5^o$ was excluded from the optimization because in this
277 range the effect of super-crystallites becomes important, which is not taken into account by
278 the code. The amount of Fe in the octahedral sheet was taken directly from the Table 1 and
279 was not optimized.
280 T_{mean} is the average thickness calculated for a lognormal distribution of crystallite
281 thicknesses. A variation of this value affects mainly the broadening of the 00l peaks.The *d*-
282 spacing represents the layer-to-layer distance of smectite structures and principally affects
283 only the positions of 00l maxima. The parameter of σ^* is a standard deviation of the Gaussian
284 orientation function of crystallites (Reynolds, 1986). The Δ-*d*-spacing describes fluctuations
285 of the layer-to-layer distance. The variations of σ^* and Δ-*d*-spacing parameters affect the
286 relative XRD intensities by a factor that is quite complex to express analytically, but is known
287 to be monotonic function of 2θ. Generally, it can be concluded that the largest modification of
288 the relative intensities of 00l reflections is influenced by the structure of interlayer species,
289 which depends on the force-fields used. This is also because all the parameters were
290 optimized to reproduce very similar values for a certain studied smectite.
291

RESULTS AND DISCUSSION

Comparison of organic force fields for EG

In order to compare the performance of organic force fields in reproducing bulk liquid EG properties, the density of a box consisting of 230 EG molecules as well as the angular distributions of the torsional O-C-C-O potential energy terms were calculated. Table 2 compares the calculated liquid densities with the experimental data. The closest agreement is achieved by the GAFF parameterization, while all other force fields result in densities noticeably lower (OPLS-aa and CGenFF) or higher (CVFF) than the experimental value.

=== Table 2 ===

The torsional O-C-C-O angle potential energy distributions were compared to a reference obtained from DFT calculations performed under the B3LYP/DGDZVP level of theory using Gaussian Inc. software package (Frisch *et al.*, 2004). In these calculations, all distances and angles were optimized for a certain O-C-C-O angle. The results (Figure 1) demonstrate that the CVFF and OPLS-aa force field parameterizations are the closest to the reference quantum chemical calculation. In the case of GAFF parameterization, the *gauche* conformation is predicted to be too stable relatively to the *trans* one. On the other hand, the stability of the *trans* conformation is overestimated in the CGenFF parameterization. All these differences are important for the proper modeling of EG conformations in smectite interlayers.

=== Figure 1 ===

317 ***Comparison of intercalate structures with 1.7 EG and 0.8 H_2O phuc***

318 The observed differences between the organic force fields, described in the previous
319 section, should have an effect on the simulated interlayer structure and resulting X-ray
320 diffraction patterns. To study this, the intercalate structure with EG and water content
321 corresponding to that of Reynolds (1965) (1.7 EG and 0.8 H_2O phuc) was calculated first. An
322 example for SWy-1 is shown in Figure 2 (the results for two other smectites are provided in
323 the supplementary materials).

324

325 === Figure 2 ===

326

327 The structures obtained using the INTERFACE and INTERFACEmod force fields are
328 substantially different than those resulting from the application of the ClayFF and ClayFFmod
329 – i.e., oxygen atoms of EG molecules have much higher tendency to be located closer to the
330 surface than their carbon atoms. In the case of the latter force fields, the positions of the
331 closest to the surface carbon and oxygen atoms do not significantly differ. A similar effect is
332 also observed for water molecules: they are located closer to the clay surface for the
333 INTERFACE- than for the ClayFF-based models.

334 Different organic force fields have also substantial effect on the resulting averaged
335 structures of the intercalate. The effect of different EG liquid density is reflected in the
336 differences in the basal spacings – the lower the density, the higher the basal spacing. There is
337 no obvious relation between the observed relative stabilities of the trans-gauche conformers
338 (Figure 1) and the obtained interlayer structures. The position of carbon atoms is relatively
339 similar for all the organic force fields tested, while there are substantial differences in the
340 positions of the oxygen atoms of EG. These differences, however, do not affect substantially
341 the calculated electron density profiles (Figure 3 and supplementary materials).

342 The modification of the Lennard-Jones parameters for the basal oxygens of smectites
343 leads to a very slight modification of the basal spacing. However, it affects the interlayer
344 structure in such a way that organic and H_2O molecules are located at somewhat larger
345 distances from the clay surface than in the original ClayFF models (Figure 2). The same
346 tendency was observed by Ferrage *et al.* (2011). These changes, in turn, affect the calculated
347 electron density profiles (Figure 3).
348
349 === Figure 3 ===
350
351 ***Comparison of intercalate structures with 0.8 H_2O phuc and basal spacing close to***
352 ***experimental***
353 Based on the structure proposed by Reynolds (1965) and on the previous MD
354 simulation studies of EG-smectite structure (Szczerba *et al.*, 2014), the content of water is
355 estimated to be around 0.8 - 1.0 molecules phuc. This value was therefore assumed as a
356 constant and chosen to be equal 0.8 phuc in the present simulations. The EG content was
357 adjusted to achieve the basal spacing close to the experimental value. This is an obvious
358 approximation due to the fact that the content of water in the structure will be related to the
359 actual relative humidity and the time between the sample glycolation and XRD measurement
360 and the conditions of the XRD profile registration. The content of water and EG is also
361 dependent on the glycolation procedure (Mosser-Ruck *et al.*, 2005). Without this
362 approximation, however, the number or necessary calculations would increase dramatically,
363 but without affecting the main conclusions too much.
364 The results of the calculations for SWy-1 are presented in Figure 4 (the results for two
365 other smectites are presented in the supplementary materials). The effect of the variation in
366 the EG content on the structures is not very strong (in comparison to Figure 2), and the main

367 factors affecting the distribution of atoms in the interlayer space are the organic force field as
368 well as the clay mineral force field.
369
370 === Figure 4 ===
371
372 ***Comparison of the calculated X-ray diffractograms***
373 In order to evaluate and further quantify the differences due to the application of
374 different organic force fields in the molecular modeling studies of organic-smectite
375 interactions, all the above calculated distributions were incorporated into the Sybilla code to
376 calculate X-ray diffractograms for the simulated structures. Thus calculated diffractograms
377 with optimized values of T_{mean}, *d*-spacing, σ^*, and Δ-*d*-spacing were then compared with
378 experimental ones (Figures 5 - 7). The results show quite significant discrepancies in the
379 obtained XRD patterns for different layer charges as well as for different combinations of
380 force fields. Because XRD is only sensitive to the distribution of electrons (the simulated
381 electron density profiles are shown in Figure 3), different electron density profiles may results
382 in different calculated XRD patterns, especially in the distribution of relative 00l intensities.
383 For low-charge montmorillonite (SWy-1; charge 0.27 phuc) the calculated results
384 agree well with experiment for all clay mineral force fields, and only relatively small
385 differences between the organic force fields used are noticeable. The modification of the
386 Lennard-Jones parameters for the basal oxygens leads to some increase of intensities of the
387 002 and 003 peaks and to a small decrease of intensities of the 004, 005 and 006 peaks.
388 For high-charge montmorillonite (SAz-1; charge 0.54 phuc) and beidellite (SbCa-1;
389 charge 0.50 phuc), the modification of the Lennard-Jones basal oxygens parameters of the
390 ClayFF-based models substantially improves the agreement between the theoretical and
391 experimental diffractograms for all the organic force fields tested. A substantial correction of

392 the 002 and 003 peak intensities towards those of experimental values is observed. A similar
393 modification applied to the INTERFACE-based models leads to only relatively small
394 improvement. This indicates that, although this force field provides a good structure for low-
395 charge montmorillonites, it should be probably modified to describe more accurately the
396 interlayer structure of high-charge smectites.
397 Among the organic force fields, the least accurate results are obtained with CGenFF.
398 This is probably related to its overestimation of the *trans* EG molecular conformation and its
399 poor agreement of the EG liquid density with experiment (Figure 1 and Table 2). Combined
400 with unmodified ClayFF, GAFF gives the best results. The resulting X-ray diffractogram is,
401 however, poor for high charge-beidellite in any combination of organic force field with
402 unmodified clay mineral set of parameters. The two other sets (OPLS-aa and CVFF) give the
403 best results for ClayFFmod. The observed differences can be related to the approximations of
404 the organic, clay mineral and water force fields and possible uncertainties in the number of
405 EG and water molecules in the interlayer estimated from experimental data and assumed in
406 the models.
407
408 === Figure 5 ===
409
410 === Figure 6 ===
411
412 === Figure 7 ===
413
414 ***Comparison of the structures with different water and EG contents***
415 Based on the results presented in the previous section, one of the two best sets of force
416 field combinations (ClayFFmod + CVFF) was used to study the interlayer structures further

and to check if the variation of the assumed EG and water content can improve the calculated X-ray diffractograms. A range of EG compositions was systematically probed between 1.4 and 2.0 phuc with a step of 0.2 phuc, with water contents varying between 0.0 and 1.2 phuc with a step of 0.3 phuc. The variation of *d*-spacing depending on the EG and water content (Figure 8) shows a plateau at around 16.5 – 17.0 Å with some further variation depending on the layer charge. Based on these plots, several structures were selected (black circles in Figure 8) to calculate average atomic distributions and then to calculate the corresponding X-ray diffraction patterns for two-layer intercalate structures.

The best of the calculated X-ray diffractograms shows only a small improvement compared to the results shown in figures 5-7 (Figure 9; all results are presented in the supplementary materials). The discrepancy between the simulated and experimental diffractograms can, therefore, be primarily attributed to the inaccuracy of the force fields used. The most important factor is clearly the selection of the clay mineral force field - its parameters may require additional improvement.

=== Figure 8 ===

=== Figure 9 ===

CONCLUSIONS

The main factor affecting the accuracy of the calculated X-ray diffractograms of EG-water intercalate in smectites is the force field selected to model clay mineral substrate. The selection of organic force field parameters, although also important, has only a secondary effect on the results obtained. The best set of parameters for smectite was found to be ClayFF with modified Lennard-Jones parameters of the basal surface oxygens (ClayFFmod). All

442 tested organic force fields perform relatively well in combination with ClayFFmod and small
443 differences between them depend on the value and location of the smectite charge. Generally,
444 among the organic force fields tested, GAFF, OPLS-aa, and CVFF perform relatively well,
445 while the application of CgenFF leads to the least accurate results.

446 The INTERFACE force field produces relatively good results for low-charge
447 montmorillonite, but it performs less well for high-charge smectites. Unlike for ClayFF,
448 modifications of the Lennard-Jones parameters for INTERFACE do not help much to
449 improve the resulting simulated X-ray diffractograms. The origin of the discrepancy between
450 the simulated and experimental diffractograms is apparently in the overestimation of the
451 interlayer atomic populations close to the clay surface.

452 Further assessment of molecular models could be performed using neutron diffraction.
453 This would, in particular, help in discriminating between models giving relatively similar
454 electron density profiles but contrasting distributions of interlayer hydrogen atoms. Using this
455 approach, positions of water molecules in the interlayer space of smectite complexes with
456 organic molecules can be much more precisely determined.

457

458 **ACKNOWLEDGMENTS**

459 This project was made possible with financial support from National Science Centre (grant
460 2012/05/B/ST10/01948), which provided IGS PAS with high-performance computing server.
461 Computer time allocations made available within the Distributed European Computing
462 Initiative (project DEC07_NUWCLAY and DEC11 COMPCLAY by the PRACE-
463 2IP receiving funding from the European Community's FP7/2007–2013 under grant
464 agreement RI-283493) and within PLGRID infrastructure are also gratefully acknowledged.
465 AGK was also supported by the industrial chair "Storage and Disposal of Radioactive Waste"
466 at the Ecole des Mines de Nantes, funded by ANDRA, Areva, and EDF.

REFERENCES

Allen, M.P., and Tildesley, D.J. (1987) Computer Simulation of Liquids. 385 p. Oxford University Press, New York.

Berendsen, H.J.C., Postma, J.P.M., van Gunsteren, W.F., and Hermans, J. (1981) Interaction models for water in relation to protein hydration. In: *Intermolecular Forces*; (B. Pullman, editor), D. Reidel: Amsterdam, pp. 331-342.

Brindley, G.W. (1966) Ethylene glycol and glycerol complexes of smectite and vermiculites. *Clay Minerals*, **6**, 237-259.

Cornell, W.D., Cieplak, P., Bayly, C.I., Gould, I.R., Merz, K.M. Jr., Ferguson, D.M. Spellmeyer, D.C., Fox, T., Caldwell, J.W., and Kollman, P.A. (1995) A second generation force field for the simulation of proteins, nucleic acids and organic molecules. *Journal of the American Chemical Society*, **117**, 5179-5197.

Cygan, R.T., Liang, J.J., and Kalinichev, A.G. (2004) Molecular models of hydroxide, oxyhydroxide, and clay phases and the development of a general force field. *Journal of Physical Chemistry B*, **108**, 1255-1266.

Cygan, R.T., Greathouse, J.A., Heinz, H., and Kalinichev, A.G. (2009) Molecular models and simulation of layered minerals. *Journal of Material Chemistry*, **19**, 2470–2481.

Dauber-Osguthorpe, P., Roberts, V.A., Osguthorpe, D.J., Wolff, J., Genest, M., and Hagler, A.T. (1988) Structure and energetics of ligand binding to proteins: E. coli dihydrofolate reductase- trimethoprim, a drug-receptor system. *Proteins: Structure, Function and Genetics*, **4**, 31-47.

Duque-Redondo, E., Manzano, H., Epelde-Elezcano, N., Martínez-Martínez, V., and López-Arbeloa, I. (2014) Molecular Forces Governing Shear and Tensile Failure in Clay-Dye Hybrid Materials. *Chemistry of Materials*, **26**, 4338-4345.

Eberl, D.D., Środoń, J., and Northrop, H.R. (1986) Potassium fixation in smectite by wetting and drying. In: *Geochemical Processes at Mineral Surfaces* (J.A. Davis and K.F. Hayes, editors), *American Chemical Society Symposium Series*, v**323**, pp. 296-326.

Eberl, D.D., Środoń J., Lee M., Nadeau P.H., and Northrop H.R. (1987) Sericite from the Silverton caldera, Colorado: Correlation among structure, composition, origin, and particle thickness. *American Mineralogist*, **72**, 914-934.

Ferrage, E., Sakharov, B.A., Michot, L.J., Delville, A., Bauer, A., Lanson, B., Grangeon, S., Frapper, G., Jimenez-Ruiz, M., and Cuello, G.J. (2011) Hydration Properties and Interlayer Organization of Water and Ions in Synthetic Na-Smectite with Tetrahedral Layer Charge. Part 2. Toward a Precise Coupling between Molecular Simulations and Diffraction Data, *Journal of Physical Chemistry C*, **115**, 1867-1881.

Frisch, M.J., Trucks, G.W., Schlegel, H.B., Scuseria, G.E., Robb, M.A., Cheeseman, J.R.T., Montgomery, J.A., Vreven, J.T., Kudin, K.N., Burant, J.C., Millam, J.M., Iyengar, S.S., Tomasi, J., Barone, V., Mannucci, B., Cossi, M., Scalmani, G., Rega, N., Petersson, G.A., Nakatsuji, H., Hada, M., Ehara, M., Toyota, K., Fukuda, F., Hasegawa, J., Ishida, M., Nakajima, T., Honda, Y., Kitao, O., Nakai, H., Klene, M., Li, X., Knox, J.E., Hratchian, H.P., Cross, J.B., Bakken, V., Adamo, C., Jramillo, J., Gomperts, R., Stratmann, R.E., Yazyev, O., Austin, A.J., Cammi, R., Pomelli, C., Ochterski, J.W., Ayala, P.Y., Morokuma, K., Voth, G.A., Salvador, P., Dannenberg, J.J., Zakrzewski, V.G., Dapprich, S., Daniels, A.D., Strain, M.C., Frakas, O., Malick, D.K., Rabuck, A.D., Raghavachari, K., Foresman, J.B., Ortiz, J.V., Cui, Q., Baboul, A.G., Clifford, S.,

512 Cislowski, J., Stefanov, B.B., Liu, G., Liashenko, A., Piskorz, P., Komaromi, I., Martin,
513 R.L., Fox, D.J., Keith, T., Al-Laham, M.A., Peng, C.Y., Nanayakkara, A., Challacombe,
514 M., Gill, P.M.W., Johnson, B., Chen, W., Wong, M.W., Gonzalez, C., and Pople, J.A.
515 (2004) *Gaussian-94, Revision C.3*. Gaussian, Inc. Pittsburgh PA.

516 Greathouse, J.A., Hart, D.B., Bowers, G.M., Kirkpatrick, R.J., and Cygan, R.T. (2015)
517 Molecular simulation of structure and diffusion at smectite-water interfaces: Using
518 expanded clay interlayers as model nanopores. *Journal of Physical Chemistry C*, **119**,
519 17126-17136.

520 Greathouse, J.A., Johnson, K.L., and Greenwell, H.C. (2014) Interaction of Natural Organic
521 Matter with Layered Minerals: Recent Developments in Computational Methods at the
522 Nanoscale, Minerals, **4**, 519-540.

523 Guillot, B. (2002) A reappraisal of what we have learnt during three decades of computer
524 simulations on water. *Journal of Molecular Liquids*, **101**, 219-260.

525 Guvench, O. and MacKerell A.D. Jr. (2008) Comparison of protein force fields for molecular
526 dynamics simulations. *Methods in Molecular Biology*, **443**, 63-88.

527 Harward, M.E. and Brindley, G.W. (1965) Swelling properties of synthetic smectite in
528 relation to lattice substitutions. *Clays and Clay Minerals*, **13**, 209-222.

529 Harward, M.E., Carstea, D.D., and Sayegh, A.H. (1969) Properties of vermiculite and
530 smectites: Expansion and collapse. *Clays and Clay Minerals*, **16**, 437-447.

531 Heinz, H., Koerner, H., Anderson K.L., Vaia, R.A., and Farmer, B.L. (2005) Force field for
532 mica-type silicates and dynamics of octadecylammonium chains grafted to
533 montmorillonite. *Chemistry of Materials*, **17**, 5658-5669.

534 Heinz, H., Lin, T.J., Mishra, R.K., and Emami, F.S. (2013) Thermodynamically consistent
535 force fields for the assembly of inorganic, organic, and biological nanostructures: The
536 INTERFACE force field. *Langmuir*, **29**, 1754-1765.

537 Heinz, H. and Ramezani-Dakhel, H. (2016) Simulations of inorganic–bioorganic interfaces to
538 discover new materials: insights, comparisons to experiment, challenges, and
539 opportunities, *Chemical Society Reviews*, **45**, 412-448.

540 Hill, J.-R. and Sauer, J. (1995) Molecular mechanics potential for silica and zeolite catalysts
541 based on ab initio calculations. 2. Aluminosilicates. *Journal of Physical Chemistry*, **99**,
542 9536–9550.

543 Humphrey, W., Dalke, A., and Schulten, K. (1996) VMD - Visual Molecular Dynamics.
544 *Journal of Molecular Graphics*, **14**, 33-38.

545 Jorgensen, W.L. and Gao, J. (1986) Monte Carlo simulations of the hydration of ammonium
546 and carboxylate ions. *The Journal of Physical Chemistry*, **90**, 2174-2182.

547 Jorgensen,W.L., Maxwell, D.S., and Tirado-Rives, J. (1996) Development and testing of the
548 OPLS all-atom force field on conformational energetics and properties of organic
549 liquids. *Journal of the American Chemical Society*, **118**, 11225-11236.

550 Kalinichev, A.G. (2001) Molecular simulations of liquid and supercritical water:
551 Thermodynamics, structure, and hydrogen bonding. *Reviews in Mineralogy &*
552 *Geochemistry*, **42**, 83-129.

553 Kalinichev, A.G., Kumar, P.P., and Kirkpatrick, R.J. (2010) Molecular dynamics computer
554 simulations of the effects of hydrogen bonding on the properties of layered double
555 hydroxides intercalated with organic acids. *Philosophical Magazine*, **90**, 2475-2488.

Kumar, P.P., Kalinichev, A. G., and Kirkpatrick, R. J. (2006) Hydration, swelling, interlayer structure, and hydrogen bonding in organolayered double hydroxides: Insights from molecular dynamics simulation of citrate-intercalated hydrotalcite. *Journal of Physical Chemistry B*, **110**, 3841-3844.

Lee, J.H. and Guggenheim, S., (1981) Single crystal X-ray refinement of pyrophyllite-1Tc. *American Mineralogist*, **66**, 350–357.

Liu, X., Lu, X., Wang, R., Zhou, H., and Xu, S. (2007) Interlayer structure and dynamics of alkylammonium-intercalated smectites with and without water: A molecular dynamics study. *Clays and Clay Minerals*, **55**, 554-564.

MacKerell, Jr. A.D., Bashford, D., Bellott, M., Dunbrack, R.L., Evanseck, J.D., Field, M.J., Fischer, S. Gao, J. , Guo, H., Ha, S., Joseph-McCarthy, D., Kuchnir, L., Kuczera, K., Lau, F.T.K., Mattos, C., Michnick, S., Ngo, T., Nguyen, D.T., Prodhom, B., Reiher III, W.E., Roux, B., Schlenkrich, M., Smith, J.C., Stote, R., Straub, J., Watanabe, M., Wiórkiewicz-Kuczera, J., Yin, D., and Karplus, M. (1998) All-atom empirical potential for molecular modeling and dynamics studies of proteins. *Journal of Physical Chemistry B*, **102**, 3586-3616.

Manevitch, O. L. and Rutledge, G. C. (2004) Elastic properties of a single lamella of montmorillonite by molecular dynamics simulation. *Journal of Physical Chemistry B*, **108**, 1428-1435.

Morrow, C.P., Yazaydin, A.Ö., Krishnan, M., Bowers, G.M., Kalinichev, A.G., and Kirkpatrick, R.J. (2013) Structure, energetics, and dynamics of smectite clay interlayer hydration: Molecular dynamics and metadynamics investigation of Na-hectorite. *Journal of Physical Chemistry C*, **117**, 5172-5187.

Mosser-Ruck, R., Devineau, K., Charpentier, D., and Cathelineau, M. (2005) Effects of ethylene glycol saturation protocols on XRD patterns: A critical review and discussion. *Clays and Clay Minerals*, **53**, 631–638.

Mukherjee, G., Patra, N., Barua, P., and Jayaram, B. (2011) A Fast empirical GAFF compatible partial atomic charge assignment scheme for modeling interactions of small molecules with biomolecular targets (TPACM4). *Journal of Computational Chemistry*, **32**, 893-907.

Ngouana Wakou, B.F. and Kalinichev, A.G. (2014) Structural arrangements of isomorphic substitutions in smectites: Molecular simulation of the swelling properties, interlayer structure, and dynamics of hydrated Cs-montmorillonite revisited with new clay models. *Journal of Physical Chemistry C*, **118**, 12758-12773.

Ortega-Castro, J., Hernández-Haro, N., Dove, M.T., Hernández-Laguna, A., and Saínz-Diaz, C.I. (2010) Density functional theory and Monte Carlo study of octahedral cation ordering of Al/Fe/Mg cations in dioctahedral 2:1 phyllosilicates. *American Mineralogist*, **95**, 209-220.

Plimpton, S. (1995) Fast parallel algorithms for short-range molecular dynamics. *Journal of Computational Physics*, **117**, 1-19.

Reynolds, R.C. (1965) An X-ray study of an ethylene glycol-montmorillonite complex. *American Mineralogist*, **50**, 990-1001.

Reynolds, R.C. (1986) The Lorentz-polarization factor and preferred orientation in oriented clay aggregates. *Clays and Clay Minerals,* **34**, 359.

600 Sato, T., Watanabe, T., and Otsuka, R. (1992) Effects of layer charge, charge location, and
601 energy change on expansion properties of dioctahedral smectites. *Clays and Clay*
602 *Minerals*, **40**, 103-113.

603 Sato, H., Yamagishi, A., and Kawamura, K. (2001) Molecular simulation for flexibility of a
604 single clay layer. *J. Phys. Chem. B*, **105**, 7990-7997.

605 Schampera, B., Solc, R., Woche, S.K., Mikutta, R., Dultz, S., Guggenberger, G., and Tunega,
606 D. (2015) Surface structure of organoclays as examined by X-ray photoelectron
607 spectroscopy and molecular dynamics simulations. *Clay Minerals*, **50**, 353-367.

608 Skipper, N.T., Refson, K., and McConnell, J.D.C. (1991) Computer simulation of interlayer
609 water in 2:1 clays. *Journal of Chemical Physics*, **94**, 7434–7445.

610 Skipper, N. T., Chang, F. R. C., and Sposito, G. (1995) Monte Carlo simulation of interlayer
611 molecular structure in swelling clay minerals. I: Methodology. *Clays and Clay*
612 *Minerals*, **43**, 285-293.
613 Smith, D.E. (1998) Molecular computer simulations of the swelling properties and interlayer
614 structure of cesium montmorillonite. *Langmuir*, **14**, 5959-5967.

615 Svensson, P.D. and Hansen, S. (2010) Intercalation of smectite with liquid ethylene glycol —
616 Resolved in time and space by synchrotron X-ray diffraction. *Applied Clay Science*, **48**,
617 358-367.

618 Suter, J.L. and Coveney, P.V. (2009) Computer simulation study of the materials properties of
619 intercalated and exfoliated poly (ethylene) glycol clay nanocomposites. *Soft Matter*, **5**,
620 2239-2251.

621 Suter, J.L., Coveney, P.V., Anderson, R.L., Greenwell, H.C., and Cliffe, S. (2011) Rule based
622 design of clay-swelling inhibitors. *Energy & Environmental Science*, **4**, 4572-4586.

623 Suter, J.L., Groen, D., and Coveney, P.V. (2015) Chemically specific multiscale modeling of
624 clay-polymer nanocomposites reveals intercalation dynamics, tactoid self-assembly and
625 emergent materials properties. *Advanced Materials*, **27**, 966-984.

626 Swadling, J.B., Coveney, P.V., and Greenwell, H.C. (2010) Clay minerals mediate folding
627 and regioselective interactions of RNA: a large-scale atomistic simulation study.
628 *Journal of the American Chemical Society*, **132**, 13750-13764.

629 Szczerba, M., Kłapyta, Z., and Kalinichev, A.G. (2014) Ethylene glycol intercalation in
630 smectites. Molecular dynamics simulation studies. *Applied Clay Science*, **91-92**, 87-97.

631 Szczerba, M., Kuligiewicz, A., Derkowski, A., Gionis, V.,Chryssikos, G.D., and Kalinichev,
632 A.G. (2016) Structure and dynamics of water-smectite interfaces: Hydrogen bonding
633 and the origin of the sharp O-Dw/O-Hw infrared band from molecular simulations.
634 *Clays and Clay Minerals*, submitted.

635 Środoń, J. (1980) Precise identification of illite/smectite interstratification by X-ray powder
636 diffraction. *Clay and Clay Minerals*, **28**, 401-411.

637 Tambach, T. J., Bolhuis, P. G., Hensen, E. J., and Smit, B. (2006) Hysteresis in clay swelling
638 induced by hydrogen bonding: accurate prediction of swelling states. *Langmuir*, **22**,
639 1223-1234.

640 Teppen, B.J., Rasmussen, K.R., Bertsch, P.M., Miller, D.M., and Schafer, L., (1997)
641 Molecular dynamics modeling of clay minerals. 1. Gibbsite, kaolinite, pyrophillite, and
642 beidellite. *The Journal of Physical Chemistry B*, **101**, 1579–1587.

643 Vanommeslaeghe, K., Hatcher, E., Acharya, C., Kundu S., Zhong, S., Shim, J., Darian, E.,
644 Guvench, O., Lopes, P., Vorobyov, I., and Mackerell, A.D. Jr. (2009) CHARMM
645 general force field: A force field for drug-like molecules compatible with the
646 CHARMM all-atom additive biological force fields. *Journal of Computational*
647 *Chemistry*, **31**, 671-90.

648 Wallqvist, A., and Mountain, R.D. (1999) Molecular Models of Water: Derivation and
649 Description. In: *Reviews in Computational Chemistry* (D.B.B. Kenny, B. Lipkowitz,
650 Eds.), v.13, p. 183-247. John Wiley & Sons, Inc., New York.

651 Wang, J., Wolf, R.M., Caldwell, J.W., Kollman, P.A., and Case, D.A. (2004) Development
652 and testing of a general amber force field. *Journal of Computational Chemistry*, **25**,
653 1157-74.

654 Wang, Y., Wohlert, J., Bergenstråhle-Wohlert, M., Kochumalayil, J. J., Berglund, L. A., Tu,
655 Y., and Ågren, H. (2014) Molecular adhesion at clay nanocomposite interfaces depends
656 on counterion hydration–Molecular dynamics simulation of
657 montmorillonite/xyloglucan. *Biomacromolecules*, **16**, 257-265.

658 Zeng Q.H., Yu A.B., Lu G.Q., and Standish R.K. (2003) Molecular dynamics simulation of
659 organic-inorganic nanocomposites: Layering behavior and interlayer structure of
660 organoclays, *Chemistry of Materials*, **15**, 4732-4738.

661
662

663 Table 1. Smectites used in the study.

Smectite	Tetrahedral charge	Octahedral charge	Fe in octahedral sheet	Particle size fraction
SWy-1	0.0	0.28	0.20	<0.1 μm
SAz-1	0.0	0.56	0.26	<2.0 μm
SbCa-1	0.50	0.0	0.09	<1.0 μm

664

665 Table 2. Comparison of calculated and experimental liquid EG density values

Organic force field	Density at 20°C (g/cm^3)
OPLS-aa	1.060
GAFF	1.123
CGenFF	1.054
CVFF	1.188
Experimental	**1.115**[a]

666 [a] The experimental value of EG density at 20°C is taken from Dow Chemicals
667 (dow.com/ethyleneglycol/about/properties.htm).
668

669

Figure 1. Potential energy scan of the torsional O-C-C-O angle of the EG molecule as reproduced by different organic force fields in comparison with quantum chemical calculations at the B3LYP/DGDZVP level of theory.

Figure 2. Z-density profile distributions for carbon and oxygen of EG, oxygen and hydrogen of water, and Ca^{2+} ions for SWy-1 for 1.7 EG and 0.8 H_2O phuc. The resulting basal spacings are also shown.

Figure 3. Electron density profiles obtained from MD simulations (black lines) compared to the profiles suggested by Reynolds (1965) (grey lines) for SWy-1 for 1.7 EG and 0.8 H_2O phuc.

Figure 4. Z-density profile distributions for carbon and oxygen atoms of EG, oxygen and hydrogen atoms of water and Ca^{2+} ions for SWy-1 with 0.8 H_2O phuc and variable EG content for which the basal spacing is close to 16.92 Å. The resulting basal spacings are also shown.

Figure 5. Comparison of **SWy-1** XRD patterns for various force field combinations (red – experimental, black – calculated).

Figure 6. Comparison of **SAz-1** XRD patterns for various force field combinations (red – experimental, black – calculated).

Figure 7. Comparison of **SbCa-1** XRD patterns for various force field combinations (red – experimental, black – calculated).

Figure 8. *d*-spacing dependence on the EG and water content for: a) SWy-1, b) SAz-1, c) SbCa-1 smectites. Small circles mark the structures which were used to calculate X-ray diffraction patterns. Thick black lines correspond to experimental basal spacings.

Figure 9. Comparison of XRD patterns for different smectites selected from the compositions in figure 8, that provide the best agreement between experimental and theoretical diffractograms.

Fig.1

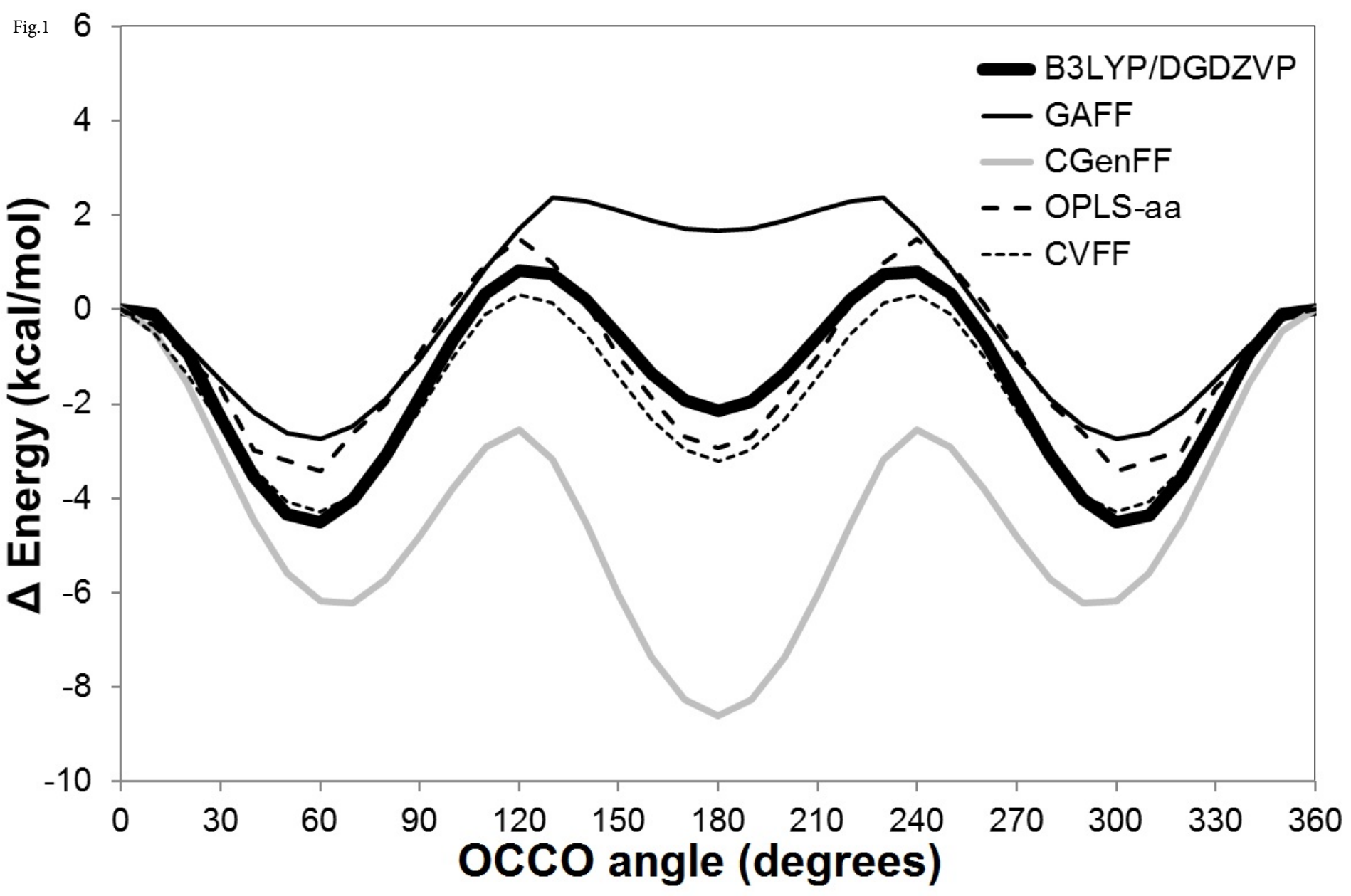
B3LYP/DGDZVP
GAFF
CGenFF
OPLS-aa
CVFF
Δ Energy (kcal/mol)
6
4
2
0
-2
-4
-6
-8
-10
0
30
60
90
120
150
180
210
240
270
300
330
360
OCCO angle (degrees)

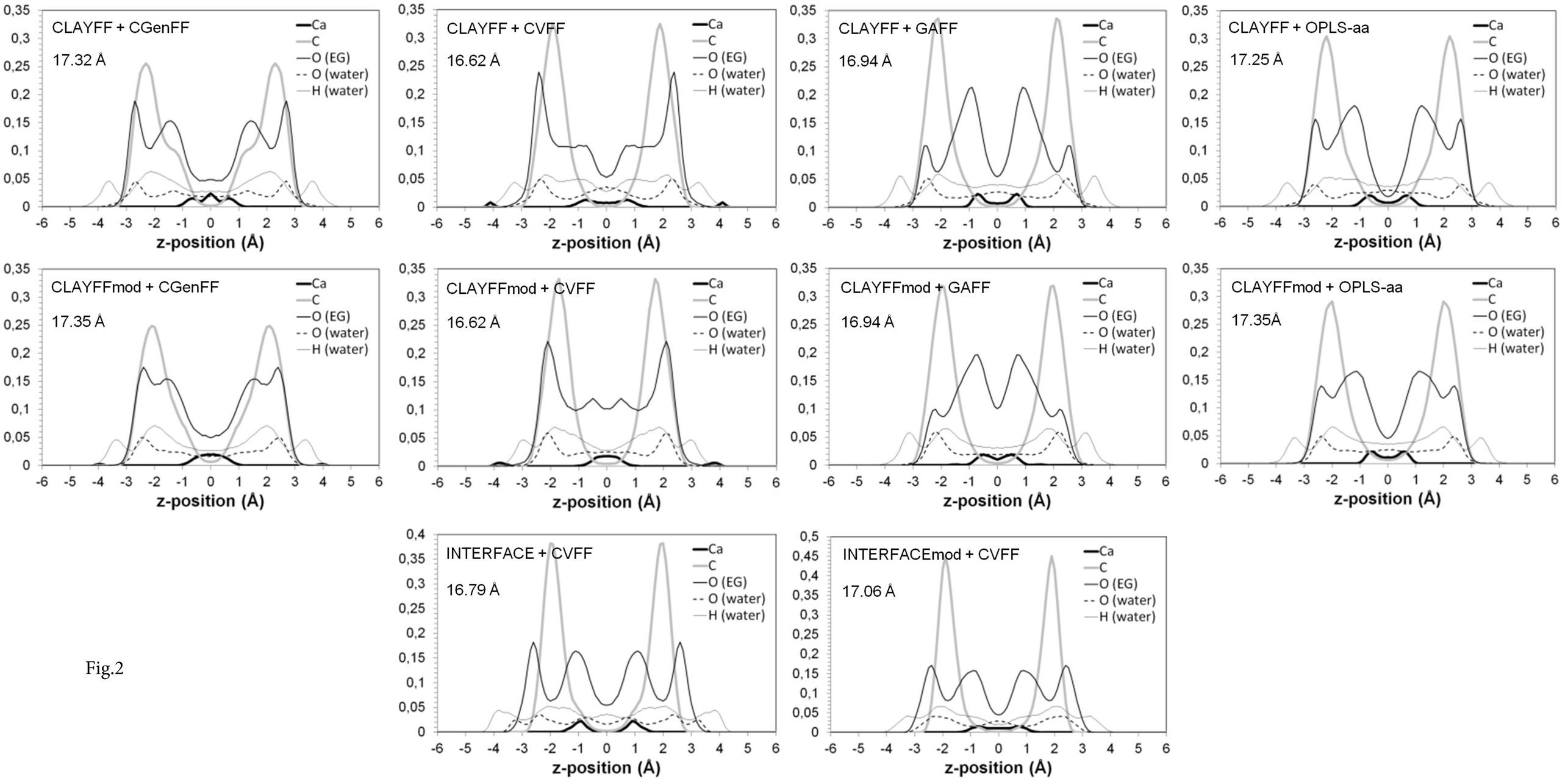
CLAYFF + CGenFF
17.32 Å
CLAYFF + CVFF
16.62 Å
CLAYFF + GAFF
16.94 Å
CLAYFF + OPLS-aa
17.25 Å
CLAYFFmod + CGenFF
17.35 Å
CLAYFFmod + CVFF
16.62 Å
CLAYFFmod + GAFF
16.94 Å
CLAYFFmod + OPLS-aa
17.35Å
INTERFACE + CVFF
16.79 Å
INTERFACEmod + CVFF
17.06 Å
Ca
C
O (EG)
O (water)
H (water)
z-position (Å)

Fig.2

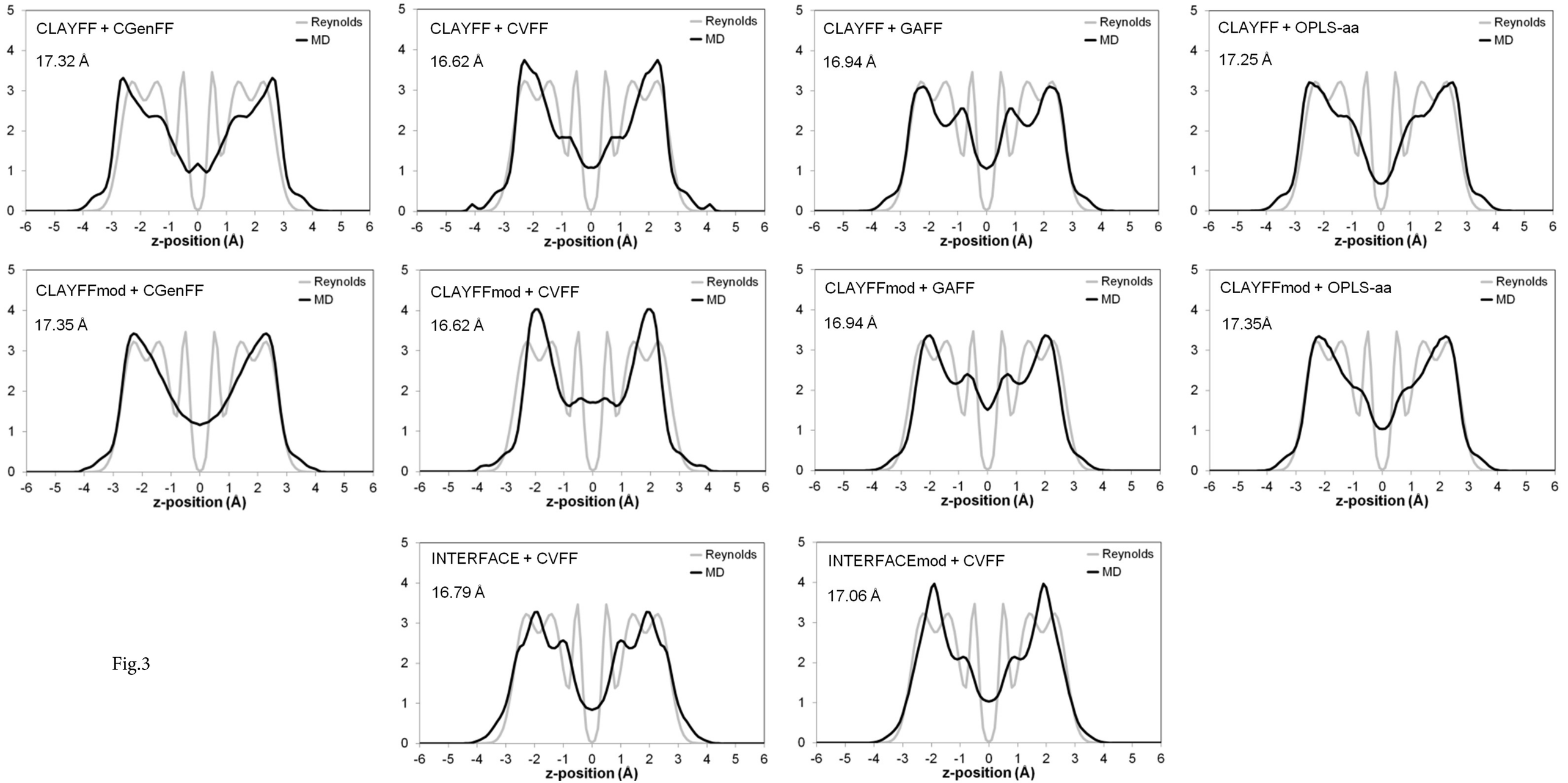
CLAYFF + CGenFF
17.32 Å
CLAYFF + CVFF
16.62 Å
CLAYFF + GAFF
16.94 Å
CLAYFF + OPLS-aa
17.25 Å
CLAYFFmod + CGenFF
17.35 Å
CLAYFFmod + CVFF
16.62 Å
CLAYFFmod + GAFF
16.94 Å
CLAYFFmod + OPLS-aa
17.35Å
INTERFACE + CVFF
16.79 Å
INTERFACEmod + CVFF
17.06 Å
Reynolds
MD
z-position (Å)

Fig.3

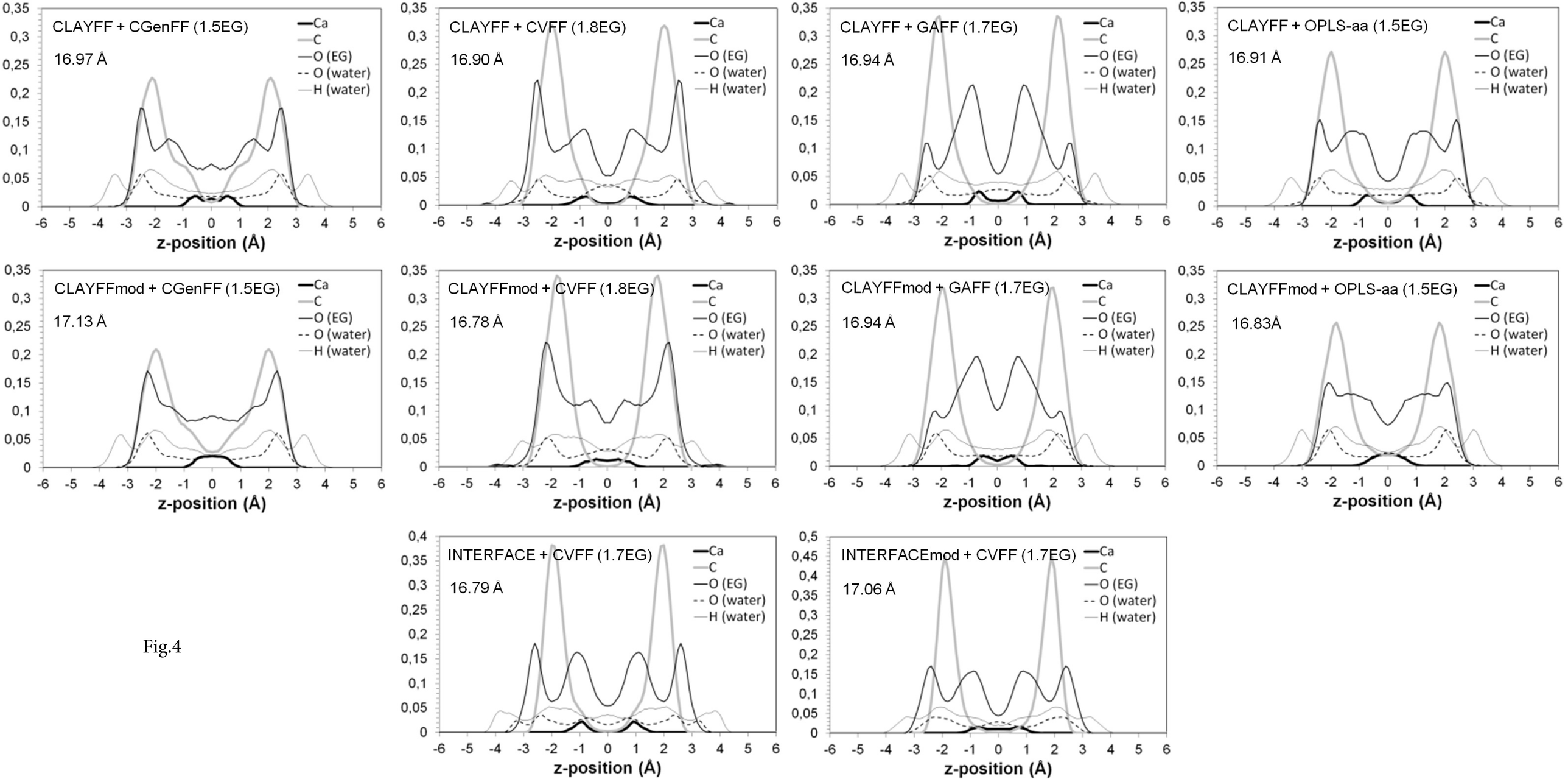
CLAYFF + CGenFF (1.5EG)
16.97 Å
CLAYFF + CVFF (1.8EG)
16.90 Å
CLAYFF + GAFF (1.7EG)
16.94 Å
CLAYFF + OPLS-aa (1.5EG)
16.91 Å
CLAYFFmod + CGenFF (1.5EG)
17.13 Å
CLAYFFmod + CVFF (1.8EG)
16.78 Å
CLAYFFmod + GAFF (1.7EG)
16.94 Å
CLAYFFmod + OPLS-aa (1.5EG)
16.83Å
INTERFACE + CVFF (1.7EG)
16.79 Å
INTERFACEmod + CVFF (1.7EG)
17.06 Å
Ca
C
O (EG)
O (water)
H (water)
z-position (Å)

Fig.4

Fig.5

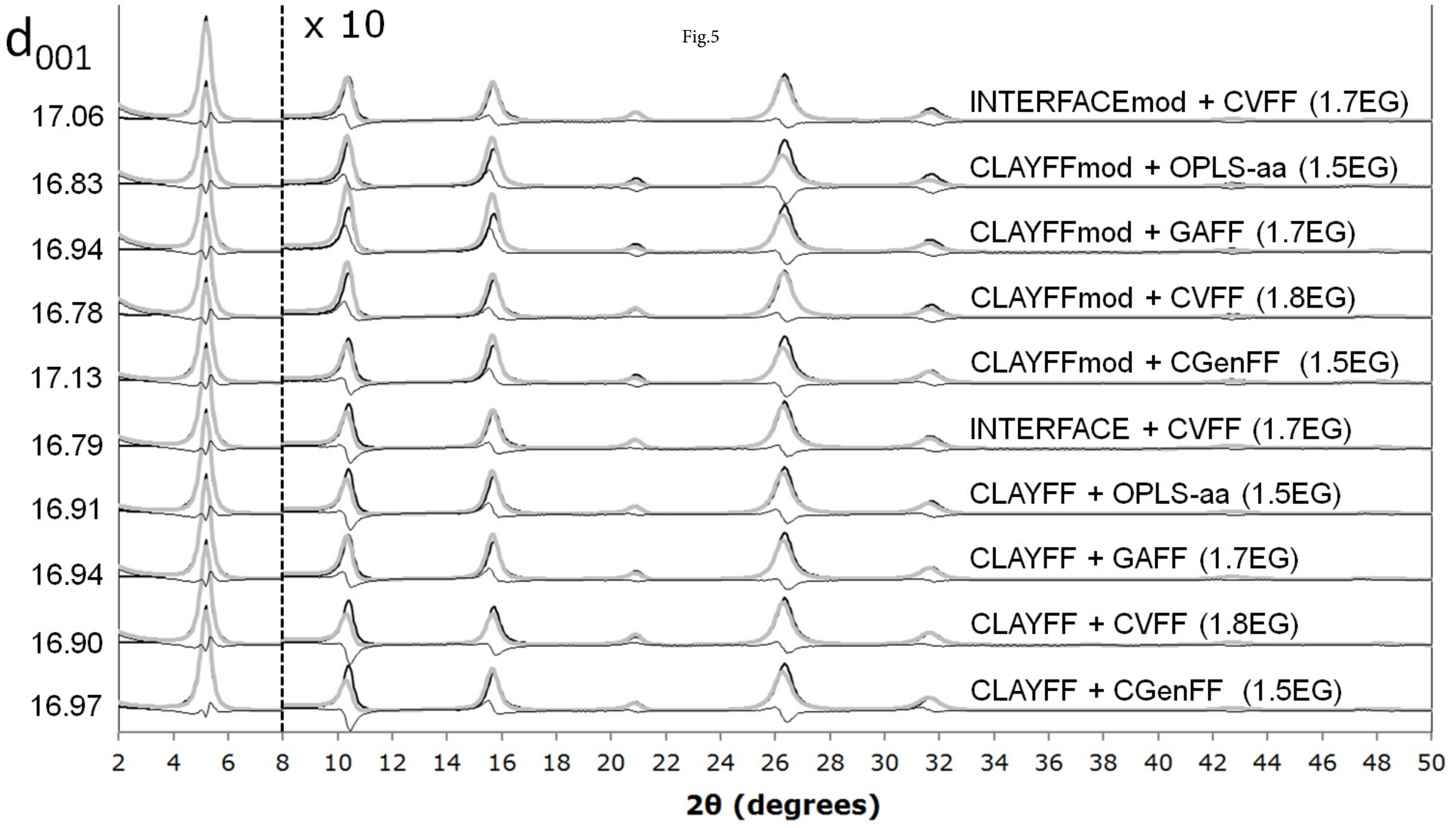
d001
x 10
17.06
16.83
16.94
16.78
17.13
16.79
16.91
16.94
16.90
16.97
INTERFACEmod + CVFF (1.7EG)
CLAYFFmod + OPLS-aa (1.5EG)
CLAYFFmod + GAFF (1.7EG)
CLAYFFmod + CVFF (1.8EG)
CLAYFFmod + CGenFF (1.5EG)
INTERFACE + CVFF (1.7EG)
CLAYFF + OPLS-aa (1.5EG)
CLAYFF + GAFF (1.7EG)
CLAYFF + CVFF (1.8EG)
CLAYFF + CGenFF (1.5EG)
2 4 6 8 10 12 14 16 18 20 22 24 26 28 30 32 34 36 38 40 42 44 46 48 50
2θ (degrees)

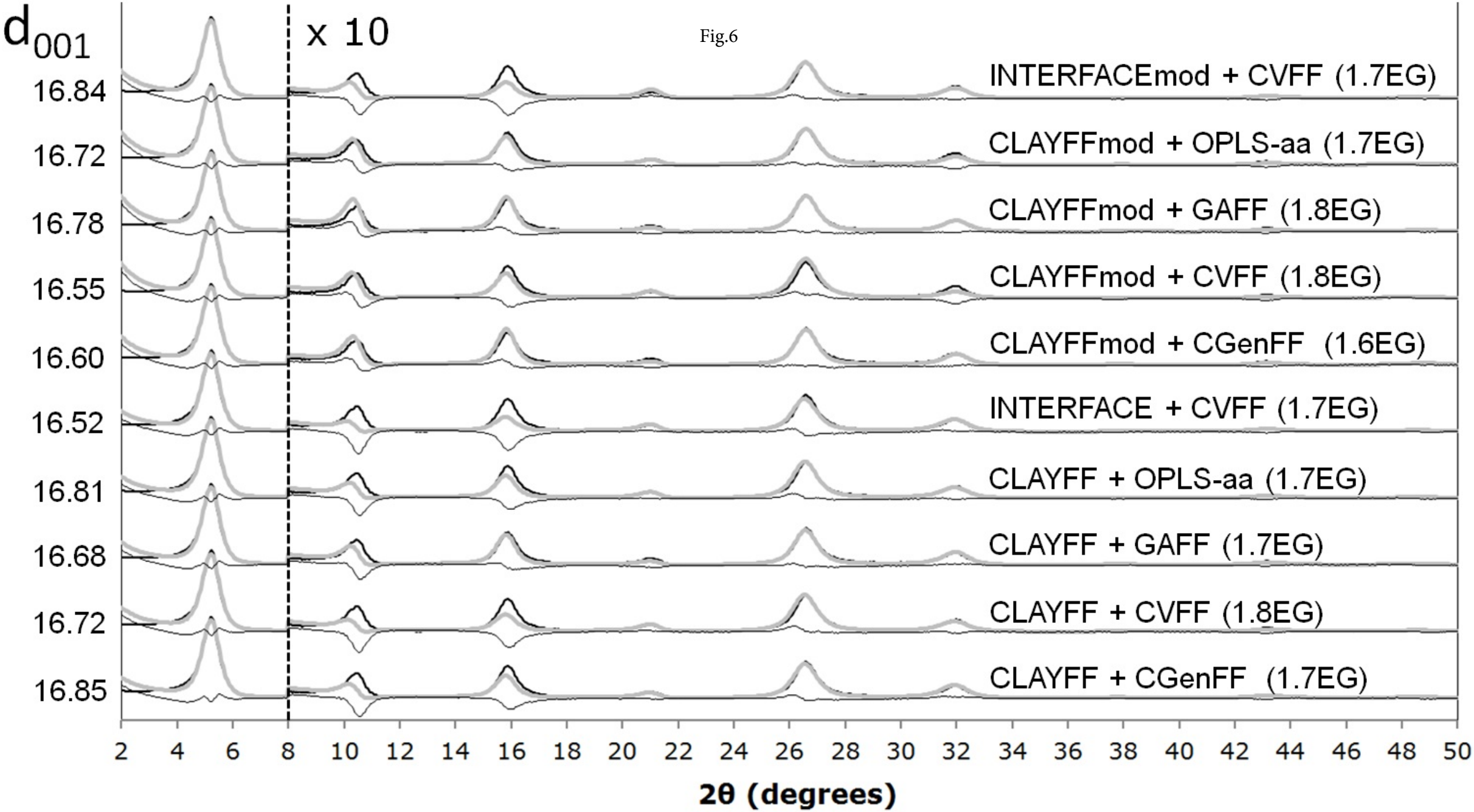
d001
x 10
16.84
INTERFACEmod + CVFF (1.7EG)
16.72
CLAYFFmod + OPLS-aa (1.7EG)
16.78
CLAYFFmod + GAFF (1.8EG)
16.55
CLAYFFmod + CVFF (1.8EG)
16.60
CLAYFFmod + CGenFF (1.6EG)
16.52
INTERFACE + CVFF (1.7EG)
16.81
CLAYFF + OPLS-aa (1.7EG)
16.68
CLAYFF + GAFF (1.7EG)
16.72
CLAYFF + CVFF (1.8EG)
16.85
CLAYFF + CGenFF (1.7EG)
2 4 6 8 10 12 14 16 18 20 22 24 26 28 30 32 34 36 38 40 42 44 46 48 50
2θ (degrees)

Fig.6

Fig.7

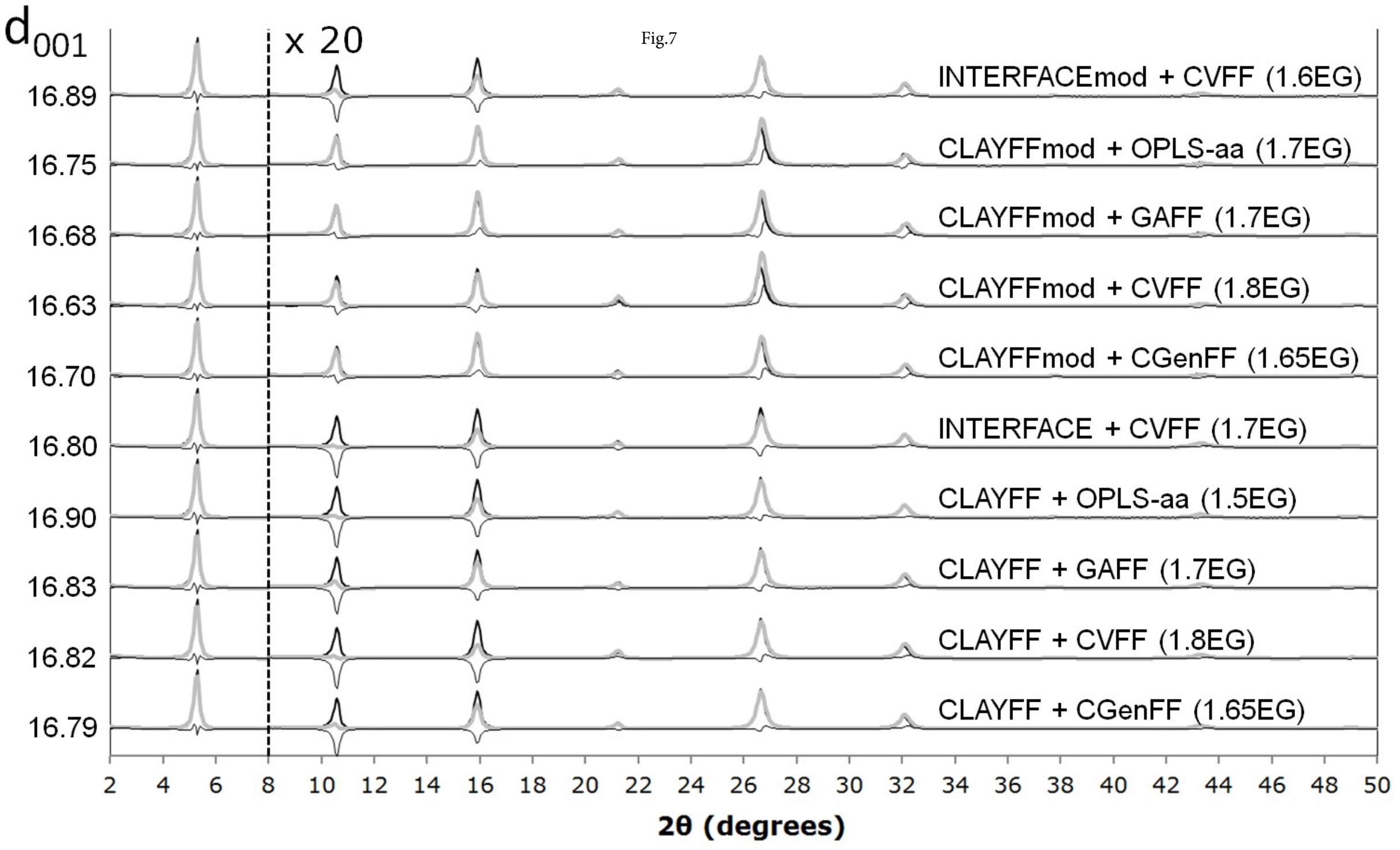
d001
x 20
16.89
16.75
16.68
16.63
16.70
16.80
16.90
16.83
16.82
16.79
INTERFACEmod + CVFF (1.6EG)
CLAYFFmod + OPLS-aa (1.7EG)
CLAYFFmod + GAFF (1.7EG)
CLAYFFmod + CVFF (1.8EG)
CLAYFFmod + CGenFF (1.65EG)
INTERFACE + CVFF (1.7EG)
CLAYFF + OPLS-aa (1.5EG)
CLAYFF + GAFF (1.7EG)
CLAYFF + CVFF (1.8EG)
CLAYFF + CGenFF (1.65EG)
2 4 6 8 10 12 14 16 18 20 22 24 26 28 30 32 34 36 38 40 42 44 46 48 50
2θ (degrees)

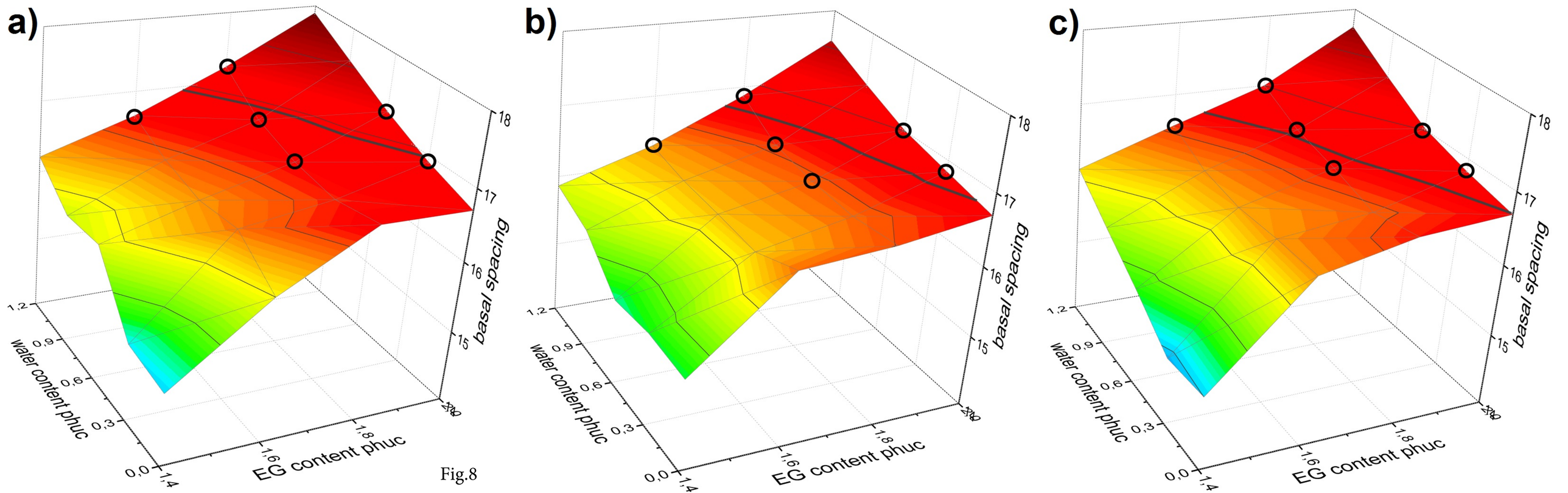
a)
b)
c)
basal spacing
15
16
17
18
water content phuc
0,0
0,3
0,6
0,9
1,2
EG content phuc
1,4
1,6
1,8
2,0

Fig.8

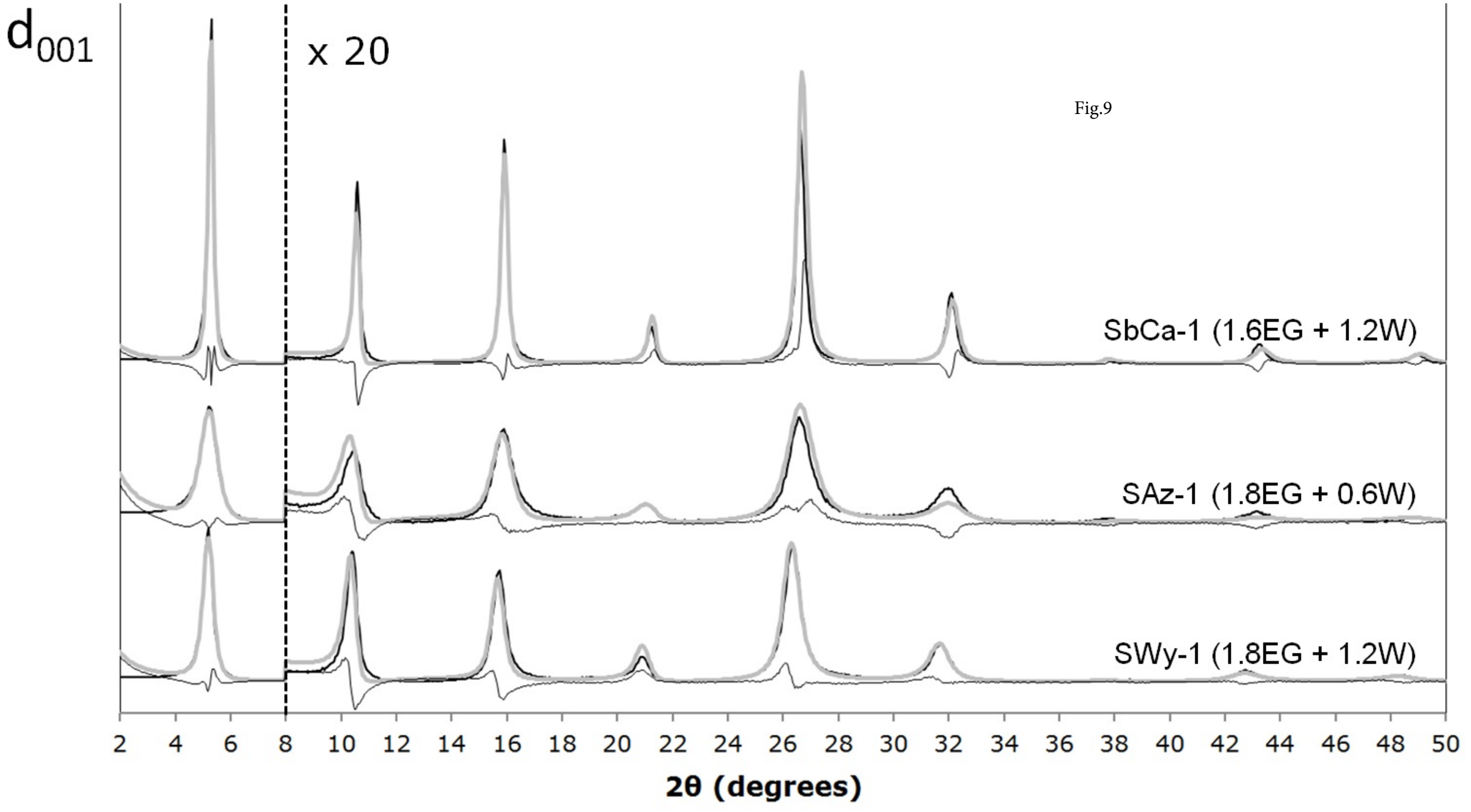
d001
x 20
SbCa-1 (1.6EG + 1.2W)
SAz-1 (1.8EG + 0.6W)
SWy-1 (1.8EG + 1.2W)
2 4 6 8 10 12 14 16 18 20 22 24 26 28 30 32 34 36 38 40 42 44 46 48 50
2θ (degrees)

Fig.9